Magnetic properties of rare-earth-based misfit layered materials of formula $(LnS)_nNbS_2$ (Ln identical to lanthanides, Y)

1991 J. Phys.: Condens. Matter 3 9929

(http://iopscience.iop.org/0953-8984/3/49/009)

J. Phys.: Condens. Matter 3 (1991) 9929–9940. Printed in the UK

Magnetic properties of rare-earth-based misfit layered materials of formula $(LnS)_nNbS_2$ (Ln ≡ lanthanides, Y)

O Peña†, P Rabu‡§ and A Meerschaut‡

† Laboratoire de Chimie Minérale B, Unité de Recherche associée au CNRS 254, Université de Rennes 1, avenue du Général Leclerc, 35042 Rennes Cédex, France

‡ IMN, Unité Mixte de Recherche Associée au CNRS 110, Laboratoire de Chimie des Solides, Université de Nantes, 2 rue de la Houssinière, 44072 Nantes Cédex 03, France

Received 29 April 1991, in final form 22 July 1991

Abstract. Crystallographic, transport and magnetic properties of several compounds of formula $(LnS)_nNbS_2$ (Ln ≡ Y, La, Ce, Nd, Sm, Gd) are presented. These compounds belong to the so-called misfit sandwiched layered phases where two-layered |LnS| and $|NbS_2|$ sublattices alternate along the *c* axis, the misfit between both sublattices occurring along the *a* axis. Single-crystal resistivities measured in the *a–b* plane present definite anomalies at $T < 2.5$ K for Ln ≡ Y, La, Ce, Sm, which could be interpreted as superconducting transitions, similar to those found, for instance, in the lead- or tin-based compounds.

Magnetic properties, essentially due to the |LnS| layers, show a wide variety of behaviours where the intrinsic anisotropy of the material is a determinant factor. The main features observed are as follows: 'local' moments due to either charge-transfer mechanisms or extrinsic effects, or both together, for Ln ≡ La; crystal-field effects and magnetic order at 1.95 K for Ce; a trivalent $^6H_{5/2}$ magnetic configuration for Ln ≡ Sm; antiferromagnetic order at $T_N = 4.6$ K for Gd; important magnetic anisotropy and crystal-field effects for Nd. Spin-flop mechanisms are apparent for the cerium and gadolinium compounds. For all lanthanides presented in this work, a trivalent state is found, in agreement with the lattice constant parameters.

1. Introduction

Numerous x-ray structure determinations of 'MTS_3' compounds, where M ≡ Sn, Pb, Bi, rare-earth metal, T ≡ Nb, Ta, have been recently reported (see the list of references in [1]). The original structural studies made on '$SnNbS_3$' [2] and '$LaNbS_3$' [3] were published at about the same time; however, the methods undertaken in the structural work were different, going from composite and/or a superspace group [4] approaches for '$SnNbS_3$' to a supercell approach for '$LaNbS_3$'. Final results led roughly to the same situation which shows that both structures are built up of alternately double layers |MS| and sandwiches $|TS_2|$; the |MS| slab is based on a distorted NaCl structure type while the $|TS_2|$ slab is of 2H–NbS_2 type (Nb in trigonal prismatic coordination). Each sublattice |MS| and $|TS_2|$ has its own symmetry (mainly orthorhombic) of F- or C-centred type.

§ Present address: IPCMS, GMI, EHICS, 1 rue Blaise Pascal, 67008 Strasbourg, France.

0953-8984/91/499929 + 12 $03.50

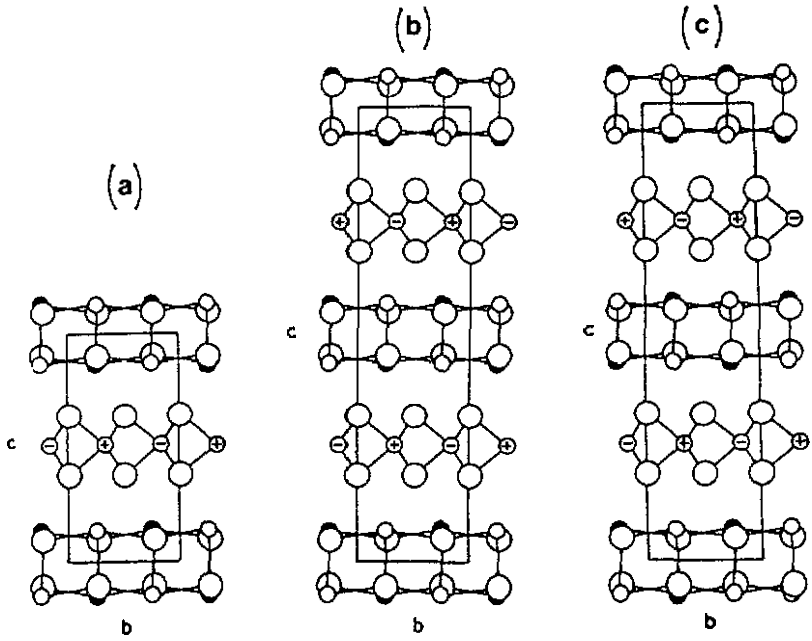

Figure 1. Structures of the three types of misfit layer compound 'MTS_3' with centred orthorhombic lattices projected along the misfit axis: (a) the CC type ($(SnS)_{1.17}NbS_2$); (b) the CF type ($(LaS)_{1.14}NbS_2$); (c) the FF type ($(PbS)_{1.13}TaS_2$). The large circles represent the sulphur atoms. T atoms in the same plane parallel to (100) have the same symbol (+ or −); atoms $\frac{1}{2}a_1$ apart have different symbols. (After Wiegers *et al* [1].)

Various situations have been reviewed by Wiegers *et al* [1] and they are illustrated in figure 1.

A new characteristic feature of such structures is given by the incommensurateness of the periodicities, leading these phases to be called 'misfit sandwiched layered phases'. Here, the lack of commensurability is defined by the a_1/a_2 ratio (where a_1 and a_2 are cell parameters along the a axis of each sublattice) which strictly determines the n-value, the chemical composition being better defined by the $(MS)_nTS_2$ formulation. The two other directions (b and c axes) are parallel and equal in length, or differ by a factor of 2. Table 1 summarizes the unit-cell parameters and the space group of some 'MTS_3' compounds.

These compounds can be regarded as resulting from the $|MS|$ layer intercalation between the $|TS_2|$ slabs. In the A_xTS_2 ternary system (A ≡ alkaline element), the intercalation process is always accompanied by a charge transfer from the intercalant to the host lattice, *i.e. the intercalant acts as a donor species*. The resulting electronic changes can be interpreted, in the rigid-band model, as the filling of the mainly 'd'-type conduction band of TS_2 [5]. The electronic transfer has been evaluated from Hall constant measurements when considering only one type of carrier. Thus, for '$LaNbS_3$', it appears that 0.88 additional electrons fill the Nb $4d_{z^2}$ band [6], which means that 0.88/1.14 (= 0.77) electrons of La are transferred to the $|NbS_2|$ part. From this calculation, it is deduced that La has a formal charge of about +2.8, which differs somewhat from the $(La^{3+}S^{2-})e^-$ scheme, characteristic of the LaS binary sulphide.

Magnetic measurements can be a complementary way to investigate these ternary systems and to confirm some results derived from the transport properties and in

Table 1. Unit-cell parameters and space groups of the two sublattices in $(LnS)_nNbS_2$ (after [5]).

		a (Å)	*b* (Å)	*c* (Å)	*β* (deg)	Space group
$(LaS)_{1.14}NbS_2$	LaS	5.828	5.797	11.52	–	*Cm2a*
	NbS_2	3.310	5.797	23.04	—	*Fm2m*
$(CeS)_{1.15}NbS_2$	CeS	5.728	5.767	11.41	—	*Cm2a*
	NbS_2	3.309	5.767	22.81	—	*Fm2m*
$(NdS)_{1.18}NbS_2$	NdS	5.635	5.742	22.663	—	*Fm2m*
	NbS_2	3.331	5.742	22.663	—	*Fm2m*
$(SmS)_{1.19}NbS_2$	SmS	5.570	5.714	22.51	—	*Fm2m*
	NbS_2	3.314	5.714	22.51	—	*Fm2m*
$(GdS)_{1.21}NbS_2$	GdS	5.518	5.71	22.53	—	*Fm2m*
	NbS_2	3.311	5.71	22.53	—	*Cm2m*
$(YbS)_{1.23}NbS_2$	YbS	5.379	5.637	22.30	—	*Fm2m*
	NbS_2	3.309	5.637	11.15	—	*Cm2m*
$(YS)_{1.23}NbS_2$	YS	5.393	5.658	22.284	—	*Fm2m*
a	NbS_2	3.322	5.662	11.13	92.62	*C2*

a Monoclinic.

particular those obtained from Hall effect studies (e.g. the number of charge carriers in '$LaNbS_3$'). In addition, since these compounds may be superconducting owing to the presence of the 2H–NbS_2 slabs (the critical temperature T_c of binary 2H–NbS_2 is 6.3 K [7]), magnetic measurements may be a useful tool for confirming a bulk superconductivity in these compounds. In the specific case of the lanthanides series (M ≡ Ln), it is also of interest to investigate the magnetic behaviour of each specific rare-earth element and the possible interactions within and in between the |MS| slabs; in particular, the intrinsic anisotropy of these layered phases will be determinant to many of the magnetic characteristics of these compounds.

In this work, after a brief recall of the sample preparation techniques and electrical resistivity results obtained in single crystals, we shall present the magnetic measurements performed in some of the compounds of the rare-earth series $(LnS)_nNbS_2$.

2. Results

2.1. Sample preparation

The $(LnS)_nNbS_2$ compounds were prepared by heating a mixture of Ln_2S_3 and NbS_2 in a 0.6:1 ratio, at a temperature of 1050 °C for 1 week in a silica tube protected by a thin film of carbon. Ln_2S_3 was previously obtained from the oxides Ln_2O_3 by sulphuration under a gas flow of H_2S–Ar at 1300–1350 °C for 4 h. Single crystals were obtained by a transport method using iodine (amount of iodine, less than 5 mg cm^{-3}).

2.2. Resistivity measurements

Electrical resistivity in the *a–b* plane was measured in single crystals of various compounds of this series [8]. The variation in the resistance *R* versus temperature indicates a metallic behaviour in the range 2.5–300 K. The resistivity values at room temperature

Table 2. Characteristic values of the resistivity of some $(LnS)_nNbS_2$ compounds.

	ρ_{ab} (290 K) (mΩ cm)	ρ_{ab} (290 K)/ρ_{ab} (5 K)	T_c [a] (K)
2H–NbS_2	0.15	—	6.3
$(LaS)_{1.14}NbS_2$	0.3	3.6	2.3
$(CeS)_{1.15}NbS_2$	0.25	2.8	2.4
$(NdS)_{1.18}NbS_2$	0.17	3.1	—
$(SmS)_{1.19}NbS_2$	—	2.2	2.4
$(GdS)_{1.21}NbS_2$	0.25	4.0	—
$(YS)_{1.23}NbS_2$	0.12	5.0	1.2

[a] Because of the large width of the transition, the onset T_c-values are approximate.

lie between 100 and 300 μΩ cm with resistance ratios in the range 2–5 (table 2). A broad variation in $R(T)$ around 2.3 K was observed in $(LaS)_{1.14}NbS_2$, $(CeS)_{1.15}NbS_2$ and $(SmS)_{1.19}NbS_2$ (figure 2). In the case of $(YS)_{1.23}NbS_2$ a slight decrease in resistance occurred at the lowest temperature of measurement. Such variations may be interpreted as superconducting transitions, similar to those found in analogous compounds [9], and which may correspond to a lowering of the critical temperature of the binary 2H–NbS_2 (table 2). In the case of $(CeS)_{1.15}NbS_2$, however, it may also be due to magnetic ordering, as discussed below and elsewhere [10].

2.3. Magnetic measurements

Magnetic measurements were performed on platelet-like single crystals or crystallized powder, using a SQUID susceptometer (SHE VTS-906) down to 1.8 K and up to 64 kOe. Powdered samples were put into a metallic holder without any preferred orientation. Single crystals were pasted onto a thin quartz rod using a GE 2051 varnish, keeping more or less parallel and perpendicular directions with respect to the magnetic field. Susceptibility measurements were performed at 1, 5 and 10 kOe, depending on the range of temperatures and after verification of the linearity of the moment M versus H. Magnetization curves were recorded at low temperatures under increasing and decreasing fields, to check for magnetic hysteresis. Contrary to the resistivity measurements, no superconducting state or diamagnetic anomalies were found in this temperature range. Different magnetic behaviours were encountered in all this series, as summarized in table 3.

2.3.1. $(YS)_{1.23}NbS_2$. A temperature-independent magnetic susceptibility, with a Curie-like tail at low temperatures ($\mu_{eff} \simeq 0.15\mu_B$ mol^{-1}) was observed in $(YS)_{1.23}NbS_2$; its high-temperature ($T > 150$ K) value is approximately $\chi \simeq 28 \times 10^{-6}$ emu mol^{-1}, a factor of 5–10 lower than the value observed for single crystals of other ternary sulphides containing non-magnetic rare-earth ions, such as the Chevrel phases $LuMo_6S_8$ or $YbMo_6S_8$ [11]. Since this value can be considered negligible compared with the magnetic contributions of all other rare earths, no correction of diamagnetic or paramagnetic temperature-independent terms was done in the following, except in the specific case of $(CeS)_{1.15}NbS_2$.

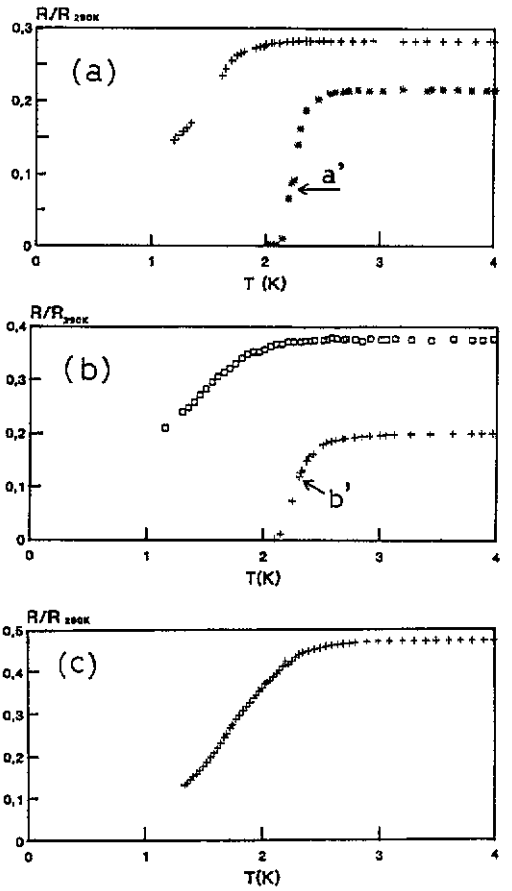

Figure 2. Single-crystal low-temperature resistivities measured in the *a–b* plane for: (a) $(LaS)_{1.14}NbS_2$; (b) $(CeS)_{1.15}NbS_2$; (c) $(SmS)_{1.19}NbS_2$. Curves denoted (a') and (b') were obtained in single crystals prepared from $Ln_2S_3 : NbS_2 = 1:1$, this being in a different ratio from that described in the text (0.6:1), and may indicate partial superconductivity.

2.3.2. $(LaS)_{1.14}NbS_2$. In the case of $(LaS)_{1.14}NbS_2$ a fairly linear temperature dependence of χ^{-1} is observed in the whole temperature range (1.85 K ≤ T ≤ 300 K). A non-negligible effective moment of approximately 0.5 μ_B is deduced, which is probably due to the partial charge transfer from $|LaS|$ to the $|NbS_2|$ sublattice, as suggested by the Hall coefficient measurements [6]. Other possible causes are presented in the discussion section.

2.3.3. $(CeS)_{1.15}NbS_2$. Crystal-field effects exist in $(CeS)_{1.15}NbS_2$. An effective moment of 2.54μ_B, which corresponds exactly to the theoretical Ce^{3+} free-ion state, is obtained above 100 K, after subtraction of a temperature-independent paramagnetic term χ_0 (figure 3). The value of χ_0 was estimated from a high-temperature χT versus T plot and it is approximately equal to 3.6×10^{-4} emu mol^{-1}. Below 10 K, an effective moment of about 1.46μ_B and a positive Curie temperature of 1.8 K are observed (inset in figure 3).

2.3.4. $(SmS)_{1.19}NbS_2$. Figure 4 shows the magnetic susceptibility of oriented $(SmS)_{1.19}NbS_2$ single crystals. A small magnetic anisotropy was observed, the preferred

Table 3. Anisotropic magnetic properties of some $(LnS)_nNbS_2$ compounds: HT, high temperature; LT, low temperature.

		μ_{eff} (μ_B)		θ (K)		
	μ_{th} (Ln^{3+})	$\perp$	//	$\perp$	//	Comments
$(YS)_{1.23}NbS_2$ non-oriented single crystals	—	$\chi_0 = 28 \times 10^{-6}$ emu mol^{-1}				Temperature-independent paramagnetism
$(LaS)_{1.14}NbS_2$ non-oriented single crystals	0		0.5		−3.5	Charge transfer [6] or extrinsic effects [10]
$(CeS)_{1.15}NbS_2$ (powder)	2.54	2.54	HT	−60	HT	$T_N = 1.95$ K
		1.46	LT	+1.8	LT	$\chi_0 = 358 \times 10^{-6}$ emu mol^{-1}
$(NdS)_{1.18}NbS_2$	3.62	3.67	3.70	−1.7	−39	HT
		3.26	2.1	0	−0.6	CEF at LT
$(SmS)_{1.19}NbS_2$	0.85	0.86 ±0.05	1.03 ±0.08	−12	−11	Van Vleck $^6H_{5/2}$ at LT
$(GdS)_{1.21}NbS_2$	7.94	7.59	7.78	−3.1	−2.3	$T_N = 4.6$ K

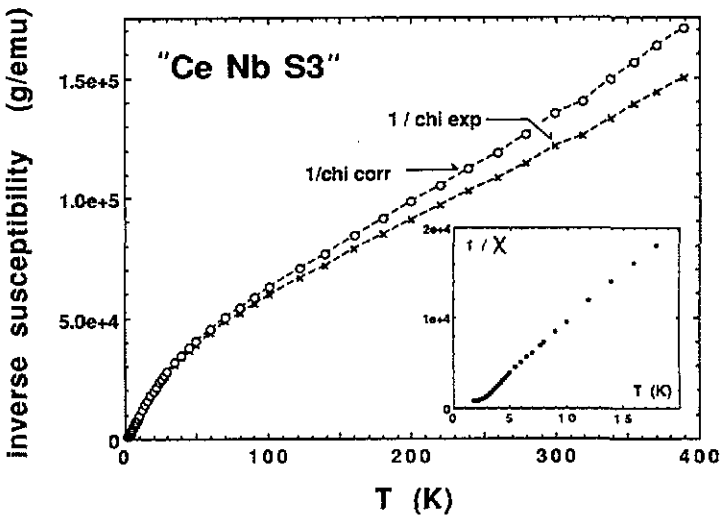

Figure 3. Inverse magnetic susceptibility of $(CeS)_{1.15}NbS_2$ sintered powder before and after correction with a temperature-independent contribution χ_0 ($=3.6 \times 10^{-4}$ emu mol^{-1}). The inset shows the magnetic ordering at low temperatures, measured under a 1 kOe magnetic field.

orientation being the *a–b* plane parallel to the magnetic field, as inferred from the magnetization curves at 5 K (inset in figure 4). Magnetic moments of 0.86 (± 0.05) μ_B and 1.03 (± 0.08) μ_B can be roughly estimated in a narrow temperature range below 12 K for the perpendicular and parallel data, respectively, which agree with a Sm^{3+} valence state.

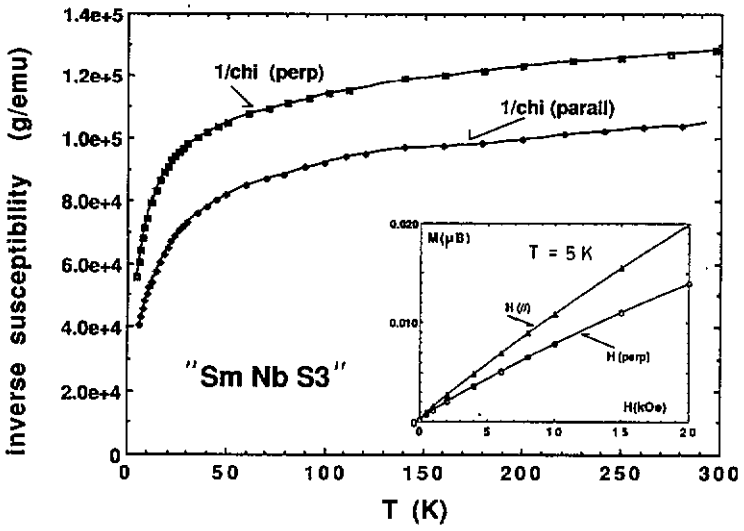

Figure 4. Inverse magnetic susceptibility of $(SmS)_{1.19}NbS_2$ single crystals oriented parallel and perpendicular to the applied field. The inset shows the magnetization at 5 K.

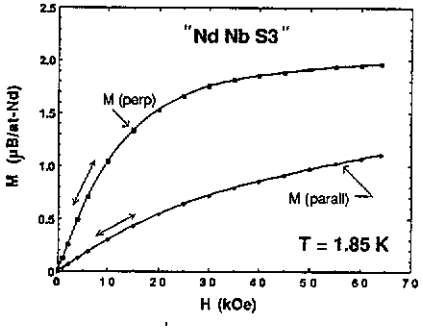

Figure 5. Magnetization at 1.85 K of oriented single crystals of $(NdS)_{1.18}NbS_2$.

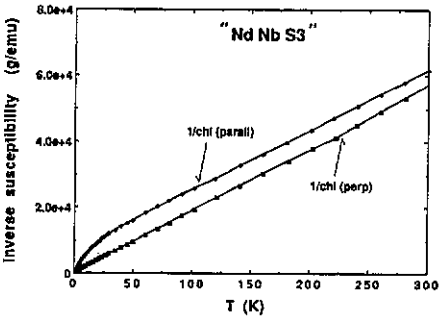

Figure 6. Inverse susceptibility of $(NdS)_{1.18}NbS_2$ single crystals oriented parallel and perpendicular to the applied field.

2.3.5. $(NdS)_{1.18}NbS_2$. A large magnetic anisotropy is observed for $(NdS)_{1.18}NbS_2$, as made evident by the magnetization curves measured at 1.85 K (figure 5). The curve saturates to $2\mu_B$ at about 60 kOe along the easy axis of magnetization (H perpendicular to the a–b plane and parallel to the c-axis), while it reaches only half of that value along the planes. Neither hysteresis nor remanent magnetization was observed. The magnetic susceptibility as a function of temperature was measured along both directions; a linear variation of χ^{-1} versus T was observed in the whole temperature range when the field was applied perpendicular to the crystal planes (figure 6). The same slope was observed for the other direction above 50 K. An effective moment close to the theoretical Nd^{3+} free-ion value was obtained above 50 K ($\mu_{exp} = 3.67\ \mu_B$ and $3.70\mu_B$, for the perpendicular and parallel directions, respectively, compared with $3.62\mu_B$ for the Nd^{3+} ion). Below

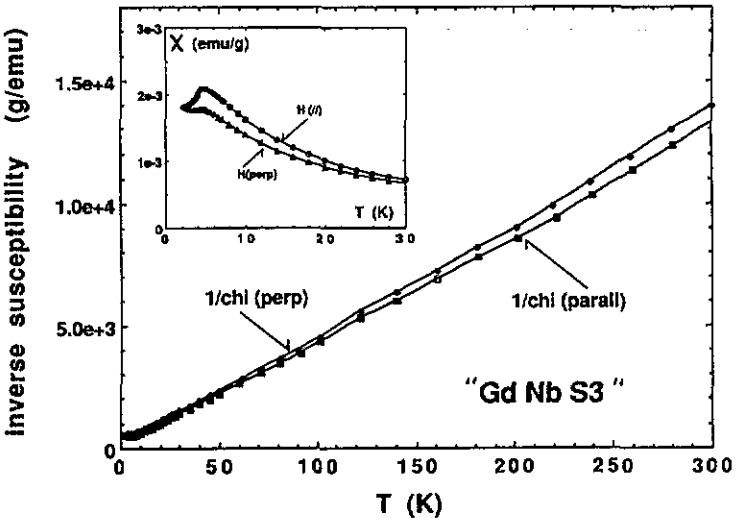

Figure 7. Magnetic susceptibility of $(GdS)_{1.21}NbS_2$ single crystals. The inset shows the magnetic order at 4.6 K.

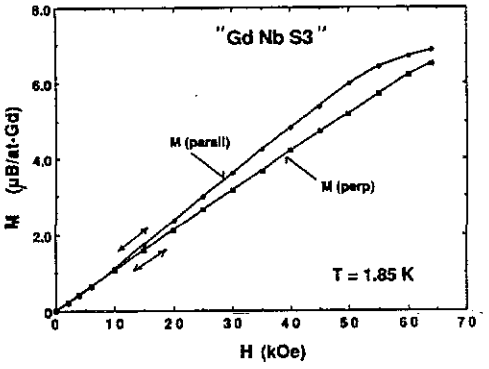

Figure 8. Magnetization at 1.85 K of $(GdS)_{1.21}NbS_2$ single crystals oriented parallel and perpendicular to the applied magnetic field.

10 K, a magnetic moment of approximately 2.1 ($\pm$ 0.05) μ_B was observed for the parallel direction.

2.3.6. $(GdS)_{1.21}NbS_2$. The reciprocal susceptibility of $(GdS)_{1.21}NbS_2$ measured at 1 kOe gives an effective moment very close to the Gd^{3+} free-ion value (7.8μ_B per Gd ion and 7.6μ_B per Gd ion for the parallel and perpendicular directions, respectively, compared with μ_{the} = 7.94μ_B), with a negative Curie–Weiss temperature between 2 and 3 K. Figure 7 shows the temperature variation in the susceptibility for both directions; almost no magnetic anisotropy is observed above 10 K. However, large differences are observed at low temperatures (inset in figure 7), and in particular a marked peak at 4.6 K for the parallel direction and a plateau for the perpendicular direction. Magnetization measurements on oriented single crystals were performed at 1.85 K, with a magnetic field applied parallel and perpendicular to the crystal planes (figure 8). Magnetization

saturates to $7\mu_B$ under 60 kOe, with a slight inflection at 10 kOe (S-shaped curve) for the parallel direction; when the field is applied perpendicular to the planes (along the *c* axis), the magnetization stays linear up to 60 kOe.

3. Discussion

The rare-earth-based misfit layered compounds presented above essentially show the theoretical magnetic moment of the lanthanide atoms in their trivalent state. A noticeable exception is, however, the $(LaS)_{1.14}NbS_2$ compound, for which the specific chemical formulation of 1.14 LaS per NbS_2 allows a partial transfer of about 0.8 valence electrons from the |LaS| sublattice to the $|NbS_2|$ part, according to Hall coefficient estimations by Wiegers and Haange [6]. Such a result was confirmed by the same workers through magnetic measurements which show that 14% of the La atoms are in a $4f^1$ state [6].

In our case, the effective moment of $0.5\mu_B$ would correspond to about 4% of 'magnetic' (cerium-like) lanthanum atoms, much less than the result obtained by Wiegers and Haange. An extrinsic origin cannot be excluded, since traces of magnetic rare-earth elements present in the starting oxides could produce similar effects. However, only part of such a magnetic moment can be attributed to extrinsic effects, since the magnetic susceptibilities of La_2O_3 (as received) and La_2S_3 showed a Curie-like tail corresponding to about $(0.15–0.18)\mu_B$. An additional hint that the paramagnetic moment observed may have an extrinsic character comes from the fact that the Curie–Weiss temperature observed in [6] was about −35 K, while in our case it is of the order of −3.5 K, implying different origins for the antiferromagnetic coupling. It should be also noted that the fairly linear *T*-dependence of the reciprocal susceptibility χ^{-1} up to 300 K may be just fortuitous if both diamagnetic (|LaS| and $|NbS_2|$ contributions) and paramagnetic Pauli susceptibility are of similar absolute values, as also assumed in [6]. Then, the overall temperature-independent contribution is negligible, as confirmed by the very low χ_0-value for $(YS)_{1.23}NbS_2$, and only the Curie–Weiss behaviour of the magnetic impurities will be seen.

Crystal-field effects are quite important in $(CeS)_{1.15}NbS_2$. The high-temperature effective moment which corresponds to the trivalent free ion implies that all six levels of the $J = \frac{5}{2}$ state are equally populated at 300 K. At low temperatures, a smaller moment $(1.46\mu_B)$ is attained, while the magnetization saturates at about $0.7\mu_B$ at 2 K [10]. Assuming that the distorted NaCl-type structure of the |CeS| slab creates a crystal field of cubic symmetry, we propose that the ground state of the cerium ion may be a Γ_7 doublet. The low-temperature susceptibility diverges at 1.8 K, indicating the existence of ferromagnetic interactions inside the |CeS| layer, while weak antiferromagnetic coupling between layers may account for the sharp maximum of χ observed at 1.95 K [10]. Such exchange interactions were also observed in the single- and double-layered cerium tantalum sulphides ($(CeS)_{1.2}TaS_2$ and $(CeS)_{1.2}(TaS_2)_2$, respectively [12]).

Antiferromagnetic interactions undoubtedly exist in $(GdS)_{1.21}NbS_2$ as evidenced by the negative Curie temperature and the maximum of χ at T_N. Exchange coupling occurs probably inside the GdS layer, since the favourable axis of magnetization lies on the *a–b* plane. When the magnetic field *H* is applied perpendicular to the crystal plates, the spins will hardly orient and the susceptibility will stay fairly constant below 4 K; the slight variation seen in the inset in figure 7 is probably due to some misorientations of the crystals with respect to the applied field. In the ordered state, the S-shaped magnetization (figure 8) is reminiscent of spin-flop mechanisms or of metamagnetic

transitions [13]; the spins would be antiferromagnetically coupled at low fields and will tend to order ferro- or paramagnetically at high fields. The very small anisotropy observed in $(GdS)_{1.21}NbS_2$ in both the susceptibility and the magnetization behaviours suggests that Gd^{3+} spins are gradually rotated upon the application of a magnetic field, as in a spin-flop transition. Much more anisotropic systems, such as the cerium analogues $((CeS)_{1.2}(TaS_2)_2$ [12] and probably $(CeS)_{1.15}NbS_2$ [10]) will show a sudden spin reversal at H_c, characteristic of metamagnetic systems. Both the saturation moment σ_s at 1.85 K ($7\mu_B$) and the effective moment μ_{eff} deduced from the Curie constants (table 3) are in full agreement with the free-ion values for trivalent gadolinium atoms.

A different situation is observed in the $(NdS)_{1.18}NbS_2$ compound. Nd^{3+} spins are mainly oriented along the *c* axis, i.e. perpendicular to the crystal platelets, and the magnetization easily saturates to $2\mu_B$ (figure 5). Only half of that value is obtained when the magnetic field is applied parallel to the *a–b* plane. The low saturation moment σ_s compared with gJ ($3.28\mu_B$), together with an effective moment of only $2.1\mu_B$ below 10 K show the importance of crystal-field effects at low temperatures. The crystal-field splitting might be of the order of 60–100 K, since the free-ion value ($3.62\mu_B$) is easily reached above 50 K for both orientations (figure 6).

The $(SmS)_{1.19}NbS_2$ compound is a typical case of Van Vleck paramagnetism where admixtures of the low-lying energy state ($J = \frac{5}{2}$) and states of higher J are expected at high temperature [14]. The effective moment calculated below 20 K (table 3) is in good agreement with a $^6H_{5/2}$ Sm^{3+} configuration ($\mu = 0.85\mu_B$). Further confirmation of the trivalent state comes from the *a* and *b* parameters of the |SmS| sublattice which follows the regular contraction of trivalent lanthanides (table 1). It is pertinent to recall the case of SmS, the well known valence fluctuating system where divalent samarium changes to a mixed valence state under hydrostatic ($P > 6.5$ kbar) or 'chemical' ($Sm_{1-x}M_x^{3+}S$) pressure (see, for instance, [15]). In our present case, the parameters *a* or *b* of the |SmS| sublattice are in close agreement with the cell parameters of a hypothetical $Sm^{3+}S$ (NaCl structure), estimated to be 5.62 Å [16], compared with 5.97 Å for the zero-pressure non-magnetic semiconducting $Sm^{2+}S$. From this comparison, we might conclude that the $|NbS_2|$ sublattice exerts a chemical pressure on the |SmS| layer, thus favouring the trivalent state of samarium, as confirmed by the magnetic results.

To end the discussion section, it is rather surprising that no signs of superconductivity were observed in our magnetic measurements, contrary to the marked anomalies in the transport properties (figure 2 and table 2). Different explanations may be considered.

(i) The remanent field (about 20–50 Oe) of the superconducting magnet has an influence, which persists during the 'zero-field' cooling or warming of the samples. However, the large H_{c_2} values of many of these compounds [9] are against this interpretation.

(ii) There is strong flux pinning in the mixed state which will preclude the detection of a Meissner effect (cooling under the remanent field), as in $EuMo_6S_8$ under pressure [17]. Pinning centres would be due to defects or grain boundaries (unlikely in the case of single crystals) or to the intrinsic composite texture of these layered materials.

(iii) Large demagnetizing factors of each 2H–NbS_2 superconducting slab are present. In this case, the critical field H_{c_1} of the first vortex penetration may be reduced by several orders of magnitude, as in superconducting thin films when oriented perpendicular to the applied fields [18]. Then, while the resistivity measurements will probe the percolation on the $|NbS_2|$ slab, the magnetic measurements will probe screening effects in which demagnetizing factors are extremely important.

Anyhow, the interplay between magnetism and superconductivity in these composite materials seems to be of different nature from that in other ternary superconductors (e.g. Chevrel phases [11] or high-T_c superconductors). Both sublattices are independently responsible for the magnetic ($|LnS|$) and transport ($|NbS_2|$) properties, and the presence of the lanthanide atom does not seem to interfere with the superconducting behaviour of the material, except for a lowering of T_c with respect to the 2H–NbS_2 binary [7]. It is, however, surprising that the cerium-based compound would show a similar or an even higher T_c than the yttrium or lanthanum counterparts (table 2). This would mean that the sublattices are completely decoupled and that no long-range correlations would exist between the magnetic slabs, contrary to our observations of rather strong magnetic coupling. It is also possible that the steep variation in $R(T)$ at 2.4 K in the cerium compound is just of magnetic origin, as suggested by the sharp maximum of the susceptibility observed at 1.95 K in powdered samples or at 2.5 K in single crystals [10]. Further magnetic and resistivity measurements should be done simultaneously on single crystals in order to solve some of these puzzling questions.

4. Conclusion

In conclusion, a large variety of magnetic behaviours has been found in the misfit layered compounds of general formula $(LnS)_nNbS_2$. Similar results have also been recently reported for the tantalum analogues $(LnS)_nTaS_2$ [19] and further confirms that the magnetic properties of these families come from the lanthanide sublattice. The two-dimensional character of these compounds is mainly responsible for the large anisotropy of their magnetic and transport properties.

A trivalent state was confirmed for all lanthanide ions, including the multiple-valenced samarium atom. $(LaS)_{1.14}(NbS_2)$ stays, however, a puzzling question, since partial charge transfer mechanisms [6] or impurity effects (10^{-3} magnetic atoms mol^{-1}) can be partly invoked to explain the local moments.

A superconducting state was inferred from resistivity measurements for Ln ≡ Y, La, Ce, Sm, but no confirmation could be given through our magnetic results. Several explanations can be forwarded, but further work is needed to confirm these results.

References

[1] Wiegers G A, Meetsma A, van Smaalen S, Haange R J, Wulff J, Zeinstra T, de Boer J L, Kuypers S, van Tendeloo G, van Landuyt J, Amelinckx S, Meerschaut A, Rabu P and Rouxel J 1989 *Solid State Commun.* **70** 409

[2] Meetsma A, Wiegers G A, Haange R J and de Boer J L 1989 *Acta Crystallogr.* A **45** 285

[3] Meerschaut A, Rabu P and Rouxel J 1989 *J. Solid State Chem.* **78** 35
Meerschaut A, Rabu P, Rouxel J, Monceau P and Smontara A 1990 *Mater. Res. Bull.* **25** 855

[4] van Smaalen S 1989 *J. Phys.: Condens. Matter* **1** 2791

[5] Friend R H and Yoffe A D 1987 *Adv. Phys.* **36** 1
Yoffe A D 1990 *Solid State Ionics* **39** 1

[6] Wiegers G A and Haange R J 1990 *J. Phys.: Condens Matter* **2** 455

[7] Frindt R F and Huntley D J 1976 *Optical and Electrical Properties of Layered Materials* ed P A Lee (Dordrecht: Reidel)

[8] Rabu P 1990 *PhD Thesis* University of Nantes

[9] Smontara A, Monceau P, Guemas L, Meerschaut A, Rabu P and Rouxel J 1989 *Fizika* **21** 201

[10] Peña O, Meerschaut A and Rabu P 1991 *J. Magn. Magn. Mater.* at press

[11] Peña O and Sergent M 1989 *Prog. Solid State Chem.* **19** 165
[12] Suzuki K, Kojima N, Ban T and Tsujikawa I 1990 *J. Phys. Soc. Japan* **59** 266
[13] Stryjewski E and Giordano N 1977 *Adv. Phys.* **26** 487
[14] Van Vleck J H 1932 *The Theory of Electric and Magnetic Susceptibilities* (London: Oxford University Press)
[15] Parks R D (ed) 1977 *Valence Instabilities and Related Narrow-Band Phenomena* (New York: Plenum)
[16] Holtzberg F, Peña O, Penney T and Tournier R 1977 *Valence Instabilities and Related Narrow-Band Phenomena* ed R D Parks (New York: Plenum) pp 507–12
Peña O 1979 *PhD Thesis* University of Grenoble
[17] Decroux M, Lambert S E, Maple M B, Woolf L D, Baillif and Fischer Ø 1985 *J. Low. Temp. Phys.* **60** 149
[18] Peña O 1991 *Meas. Sci. Technol.* **2** 470
[19] Suzuki K, Enoki T and Imaeda K 1991 *Solid State Commun.* **78** 73
[20] Wiegers G A and Meerschaut A 1991 *J. Less-Common Met.* **78** 73